Second-harmonic spectroscopy of a Si(001) surface during calibrated variations in temperature and hydrogen coverage

J. I. Dadap,* Z. Xu,† X. F. Hu, and M. C. Downer
Science and Technology Center for Synthesis, Growth, and Analysis of Electronic Materials, Department of Physics, The University of Texas at Austin, Austin, Texas 78712

N. M. Russell‡ and J. G. Ekerdt
Science and Technology Center for Synthesis, Growth, and Analysis of Electronic Materials, Department of Chemical Engineering, The University of Texas at Austin, Austin, Texas 78712

O. A. Aktsipetrov
Department of Physics, Moscow State University, Moscow 119899, Russia

(Received 14 July 1997)

The epitaxial growth of silicon films by chemical vapor deposition (CVD) is strongly affected by temperature and hydrogen (H) termination. We report measurements of p-polarized optical second-harmonic (SH) spectra generated in reflection from clean 2×1-reconstructed and H-terminated epitaxial Si(001) surfaces with no intentional doping by Ti:sapphire femtosecond laser pulses for SH photon energies $3.0\leqslant 2\hbar\omega\leqslant 3.5$ eV near the bulk E_1 resonance. Temperatures were varied from 200 to 900 K and H coverages from 0 to 1.5 monolayers (ML). Increases in temperature at fixed H-coverage redshift and broaden the E_1 resonance, as observed in linear bulk spectroscopy. Increases in H coverage from 0 to 1 ML at fixed temperature strongly quench, redshift, and distort the lineshape of the E_1 resonance even though reflection high-energy electron diffraction shows that the surface maintains the dimerized 2×1 reconstruction. The latter spectroscopic variations cannot be explained by vertical strain relaxation in the selvedge region, nor by bulk electric-field-induced SH (EFISH) effects. We instead attribute these variations to a monohydride-induced surface chemical modification, which we parametrize as a surface EFISH effect because submonolayer H strongly alters surface electric fields by redistributing charge from surface dimers into the bulk. The effects of vertical strain relaxation are weakly evident as a blueshift of the E_1 resonance accompanying dihydride termination (1.0–1.5 ML), which breaks the surface dimer bond. This modification is parametrized as a separate field-independent alteration to the surface dipole susceptibility $\chi^{(2)}_{\mathrm{surface}}$. Finally, guided by these SH spectroscopic studies, we demonstrate dynamic real-time (100-ms resolution) SH monitoring of H coverage (5% accuracy) during temperature programmed hydrogen desorption and CVD epitaxial growth of silicon from disilane. [S0163-1829(97)07144-0]

I. INTRODUCTION

The interaction of hydrogen with silicon surfaces is of particular importance to the chemical vapor deposition (CVD) chemistry of silane and disilane; the hydrogen desorption rate places a fundamental upper limit on the growth rate at any temperature in the absence of gas-phase reactions. Although it has been suggested as early as 1963 (Ref. 1) that hydrogen desorption limits the CVD growth rate from silane under certain conditions, it was not until kinetic studies of the monohydride desorption were performed[2,3] that the similarity in the apparent activation barriers for low-temperature CVD growth and monohydride desorption was recognized. Well-known work on the reconstruction and electronic structure of bare and hydrogen-atom-exposed, singular surfaces of silicon[4–8] has established that hydrogen forms both a monohydride and a dihydride phase on silicon. A fairly complete structural picture of the hydrogen/Si(100) system has emerged, largely as a result of the work of the following: Feldman, Silverman, and Stensgaard,[9] showed the H-saturated (100) surface has a coverage Θ_{H} of 1.5 ML; Chabal[6] demonstrated that the saturated phase consists of a mixture of monohydride and dihydride; and Boland[8] showed that domains of dihydride (with a local coverage of 2 ML) and monohydride are present at saturation. The relevance of these studies under ultrahigh vacuum (UHV) conditions to CVD growth has recently been questioned by the work of Greenlief and Armstrong,[10] which has shown significant differences between the hydrogen desorption kinetics under CVD growth conditions and UHV conditions. A surface-sensitive probe capable of operating at elevated pressures may prove particularly useful in divining the nature of such discrepancies.

Optical second-harmonic (SH) and sum frequency (SF) spectroscopy offer unique advantages as noninvasive probes of clean and hydrogen-covered silicon surfaces.[11–17] Optical probes, unlike electron-beam probes, are unperturbed by ambient gases, and thus can monitor the H-Si surface in real time during homoepitaxial and heteroepitaxial growth[11,12] by CVD. Moreover for centrosymmetric materials like Si, the second-order nonlinear optical response, unlike the linear optical response (e.g., in ellipsometry or infrared absorption), includes a highly surface-specific electric dipole component, but contains no bulk electric dipole component.[18] Unlike reflectance-difference (-anisotropy) spectroscopy (RDS/RAS),[19] the surface specificity of second-harmonic

0163-1829/97/56(20)/13367(13)/$10.00 © 1997 The American Physical Society

generation (SHG) does not depend on surface anisotropy, and thus can be applied to isotropic surfaces such as the oriented double-domain Si(001)-2×1 surface used in the present study. SHG and SFG on silicon have thus been shown to be highly sensitive to hydrogen adsorption, desorption, and diffusion kinetics,[13,20] surface structural phase transitions,[14,21,22] and temperature-dependent changes in vibrational[15] and electronic[16] surface spectra.

Nevertheless nonlinear spectroscopy of H-Si surfaces remains in a primitive state for several reasons. First, most previous SH studies have been performed at a single fixed wavelength of either 1064 or 532 nm (Refs. 11–14 and 16) corresponding to the fundamental and frequency-doubled output of pulsed Nd:YAG lasers. In such studies, surface spectroscopic information is either lacking, or at best acquired indirectly through temperature variation of the band structure,[16] which simultaneously changes other surface properties. Moreover, the quantitative relation between the SH signal and hydrogen coverage can usually be established only over limited coverage ranges at these wavelengths (e.g., 0–0.15 ML with 1.06-μm fundamental[13]). Secondly, in the only spectroscopic SH study of H-terminated Si(001) surface to our knowledge, [17] only one uncalibrated near-saturation coverage and one temperature were examined. Surface spectroscopic consequences of incremental variations in Θ_H and temperature, even though accompanied by significant changes in atomic and electronic surface structure, remain undocumented. Thirdly, acquisition of SH and SF data from the technologically important, but weakly nonlinear, Si(001) surface, has been slow and laborious because of low SHG and SFG efficiencies obtainable with long-pulse, low-repetition-rate laser sources. This in turn has limited the number of surface parameters that could reasonably be varied, as well as the speed of kinetic processes that could be monitored in real time.

In this paper, we present measurements of the spectrum of SH radiation generated in reflection from Si(001) surfaces as a function of systematically varied temperature and Θ_H by a tunable femtosecond Ti:sapphire laser. The ultrashort pulse duration ($\tau \sim 10^{-13}$ s) of such lasers permits us to deliver high focused peak light intensity ($I \sim 10^{10}$ W/cm^2) to the surface with low pulse energy ($E \sim 10^{-8}$ J), thus maximizing SH efficiency ($I_{2\omega} \sim I^2$) while minimizing surface heating ($\sim E$).[23,24] In addition, their wide continuous wavelength ($0.7 < \lambda < 1.0\ \mu$m) tunability permits broadband spectroscopy of the Si(001) surface and immediate subsurface region in the vicinity of the two-photon E_1 resonance. We present spectroscopic SH results, obtained with the p-in/p-out polarization configuration, for Si(001) surfaces under both isothermal and/or isosteric (constant H coverage) conditions and under transient conditions. On isothermal and/or isosteric surfaces we track the redshifting and broadening of the two-photon E_1 resonance for both clean Si(001)-2×1 reconstructed and H-Si(001) surfaces as temperature increases at fixed Θ_H. Our extracted temperature coefficients agree quantitatively with previous bulk linear spectroscopic analyses of thermal narrowing of the $\Lambda_3 \rightarrow \Lambda_1$ direct gap electronic transitions responsible for the E_1 resonance.[25] In addition, we measure the redshifting, quenching, and line-shape distortion of this resonance as Θ_H increases at fixed temperature. Here our results necessitate an interpretation markedly different from previous interpretations of far less complete SHG data,[17] which assumed that H termination changed the SH spectrum exclusively via relaxation of subsurface tensile strain. Our results show that the strongest observed alterations of the E_1 resonance occur for submonohydride coverage $0 \leqslant \Theta_H \leqslant 1$ ML, for which strain relaxation is much smaller than for dihydride coverage $\Theta_H > 1$ ML.[26] Moreover, monohydride-induced alterations to the bulk band bending and accompanying bulk electric-field-induced (EFISH) contributions,[27] though clearly evident in heavily doped samples,[28] can be ruled out in the present work because of the negligible space-charge field (<1 kV/cm) in our undoped samples. Our results instead suggest that monohydride-induced redistribution of charge, and thus electric field, between the surface dimers of the 2×1 reconstruction and the underlying 2–3 atomic layers—i.e., surface EFISH—plays a major role in the SH spectroscopy, as recently suggested by Xu *et al.*[28] and Aktsipetrov *et al.*[28] More subtle spectroscopic consequences of dihydride-induced strain relaxation on the surface contribution become weakly evident only for $\Theta_H > 1$ ML. In addition, we demonstrate that optical interference[29] between the resonant E_1 and the nonresonant background contributions to SHG redshifts and distorts the line shape of the E_1 feature when these two contributions become comparable in magnitude. These results are timely in view of recent theoretical advances in the calculation of surface nonlinear optical spectra,[30–32] and should stimulate new calculations of the SH spectrum of H-Si(001). Meanwhile, these isothermal and/or isosteric spectroscopic studies provide guidance for real-time SH monitoring of Si(001) surfaces during transient processes such as temperature-programmed desorption (TPD) of hydrogen. At strategically chosen wavelengths, SHG tracks the β_2 (dihydride) and β_1 (monohydride) desorption features, which are independently monitored by a quadrupole mass spectrometer (QMS) during TPD. Finally, we demonstrate that SHG at these wavelengths can be used to monitor instantaneous H coverage during epitaxial growth by CVD, allowing the hydrogen desorption kinetics during epitaxial growth to be estimated.

II. EXPERIMENTAL PROCEDURE

The SH spectroscopy experiments were performed in an ultrahigh vacuum (UHV) deposition chamber, equipped with a quadrupole mass spectrometer (QMS) and a reflection high-energy electron diffraction (RHEED) apparatus. The deposition chamber is adjoined via a load-lock to a multitechnique surface analysis chamber (base pressure 8×10^{-11} Torr) with capabilities for Auger electron spectroscopy (AES), x-ray photoelectron spectroscopy (XPS), TPD, and high-resolution electron-energy-loss spectroscopy (HREELS), which has been described elsewhere.[33] The deposition chamber is pumped by a 450-1/s turbomolecular pump to a base pressure $<1 \times 10^{-9}$ Torr (the low-pressure limit of the Bayard-Alpert gauge), with no special provisions for pumping hydrogen, because of its low[34] ($<10^{-6}$) initial sticking coefficient on Si(100). This chamber is also equipped with a Roots blower, capacitance manometer, and exhaust valve for operation at pressures up to 100 Torr. The deposition chamber is routinely exposed to large doses of

silane and disilane during CVD growth, which helps maintain a low H_2O partial pressure (via gettering at the chamber walls) of approximately 5×10^{-11} Torr, estimated from residual gas analysis. The bare silicon surface can be maintained for about 15 min under these conditions without any accumulation of impurities detectable by XPS and TPD (<0.01 ML). A typical SH spectrum was acquired in approximately 3 min (*vide infra*).

The oriented p-type Si(001) substrate (miscut less than 1°) was radiantly heated from the backside with a pyrolytic boron nitride (PBN) encased graphite heater for temperatures less than 1050 K. For higher temperatures, a coiled tungsten filament was inserted between the PBN heater and the backside of the crystal (using a linear motion device) to achieve electron beam heating to temperatures as high as 1400 K. Temperature was routinely monitored via a thermocouple, mounted to the sample holder, that was previously calibrated to the crystal temperature (to within ± 20 K). To achieve better accuracy in the temperature measurement (to within ± 5 K), all of the experiments reported here used a K-type thermocouple, spot welded to the inside of a thin roll of tantalum foil, then inserted into a 0.5-mm hole through the crystal and fastened with a drop of zirconia-based adhesive (Aremco, Ultratemp 516). The native oxide was removed as SiO by 1-K/s heating to 1275 K, followed by 1-K/s cooling to ambient. This procedure has been shown to produce an atomically smooth 2×1 reconstructed surface[8] as verified by a characteristically sharp, streaky RHEED pattern, with no impurities detectable by XPS and AES.[35] Our SH measurements were performed on an undoped, epitaxial silicon layer that was grown by UHV-CVD using disilane (Airco, electronic grade mixture consisting of 4%-Si_2H_6/balance He) at 900 K to bury any trace contaminants present at this surface, and conceal the initial interface far beyond the extinction length of the SH radiation (typically a 0.3-μm layer was grown). As surface contaminants accumulated over the course of several days, the epitaxial growth procedure was routinely repeated to recover a pristine surface, with no degradation in the crystallinity nor surface roughness, as monitored by the RHEED pattern.

Hydrogen coverage was controlled by exposing the bare crystal to atomic hydrogen produced by cracking molecular hydrogen on a 2000-K tungsten filament, placed in line-of-site with the crystal face at a distance of 3–4 cm. The hydrogen (Matheson, UHP) was purified by slowly filling an evacuated, liquid-nitrogen-cooled U tube to a pressure of 50 psi (gauge), before backfilling the chamber to the desired pressure, resulting in an H_2O partial pressure rise in the chamber to no more than 2×10^{-10} Torr at hydrogen pressures as high as 5×10^{-4} Torr. A resistively heated crystal and a line-of-site QMS were installed in the deposition chamber to quantify hydrogen coverages by TPD, while the SH spectroscopy experiments were performed concurrently on the same crystal. By normalizing the m/e 2 TPD peak areas to the area under the saturated monohydride peak, hydrogen coverages in ML were obtained with a relative accuracy of approximately 5%. Cracking of background impurities (CO, H_2O) was minimized by keeping the filament hot for no more than 30 s for each dose and varying the pressure to control the exposure. A 15 000 L (5×10^{-4} Torr, 30 s) molecular hydrogen exposure produced a saturation coverage of 1.5 ML at 375 K. Hydrogen exposure was performed at no less than 375 K to minimize the formation of etch products that might lead to surface roughening.[36] Following each exposure and SH spectroscopy experiment, the TPD heating program annealed the crystal at 1050 K to recover the smooth, double-domain (2×1)-reconstructed surface.

Unamplified Ti:sapphire laser pulses of duration 120 fs, wavelength range 705–935 nm, spectral bandwidth 5–10 nm [full width at half maximum (FWHM)], average power 150 mW, and repetition rate 76 MHz were focused through a fused-silica viewport onto the (001)-oriented silicon crystal *in vacuo* at a 55° angle of incidence. The reflected SH signal was monitored through a second optical port using a gated photon-counting system. A fraction of the fundamental laser beam was split off outside the chamber to generate a SH reference signal from a crystalline quartz plate, which normalized against drifts in average laser power or pulse duration during data acquisition. Transient surface heating by individual laser pulses was negligible (<0.5 K at 0.5 mJ/cm^2 per pulse). However, cumulative surface heating by the 76-MHz pulse train caused a steady-state temperature difference as high as 40 to 50 K (Ref. 23) between the sampled spot on the crystal and the thermocouple, mounted several mm away, when the laser operated at 200 mW average power. This extra heating noticeably perturbed H desorption kinetics, which provided *in situ* calibration of the temperature offset, as discussed in Sec. IV. Attenuation of the incident beam to <50 mW with neutral density filters minimized laser-induced heating while maintaining adequate SH signal levels for most measurements.

Two types of SH measurement are reported: (1) isothermal and isosteric spectroscopic measurements and (2) real-time fixed wavelength measurements during heating, hydrogen desorption, and epitaxial growth (time resolution <0.1 s). For surface spectroscopy, the laser wavelength was tuned between 705 and 820 nm in pulse bandwidth (5–10 nm) increments in less than 3 min, yielding a two-photon spectral energy resolution $2\hbar\Delta\omega\sim0.02-0.03$ eV. With a change in laser optics, the longer wavelength range from 800 to 935 nm was scanned in a similar manner. Spectral scans were repeated with increasing, then decreasing wavelengths to verify that contaminant adsorption did not influence the SH spectroscopy measurements during data acquisition. Periodic RHEED and XPS measurements indicated no appreciable contamination even after performing experiments for several days.

III. PHENOMENOLOGICAL FRAMEWORK

The two major sources of nonlinear polarization $\mathbf{P}^S(2\omega)$ responsible for generating SH radiation from the undoped Si(001)-2×1 surface will be expressed as

$$\mathbf{P}^S(2\omega)=\overleftrightarrow{\chi}_s^{(2)}:\mathbf{E}(\omega)\mathbf{E}(\omega)+\overleftrightarrow{\chi}_s^{(3)}:\mathbf{E}(\omega)\mathbf{E}(\omega)E_{\rm dc}^{\rm surf}, \quad (1)$$

where $\mathbf{P}^S(2\omega)$ has been related to the fundamental electric field $\mathbf{E}(\omega)$ and an effective surface dc field $\mathbf{E}_{\rm dc}^{\rm surf}=E_{\rm dc}^{\rm surf}\mathbf{z}$ (Ref. 28) via the second-order surface dipole ($\overleftrightarrow{\chi}_s^{(2)}$) and third-order surface ($\overleftrightarrow{\chi}_s^{(3)}$) nonlinear susceptibility tensors, where $\mathbf{z}$ is a unit vector normal to the surface. Both terms describe sources localized at the surface, generally including several

subsurface atomic layers, and possessing macroscopic C_{4v} symmetry as well as isotropic dependence on azimuthal crystal rotation for Si(001).[37] Surface fields $E_{\rm dc}^{\rm surf}>10^3$ kV/cm arise within the top few atomic layers of the clean 2×1-reconstructed surface because the formation of surface dimers, even symmetric ones, induces electron transfer from the bulk into the uppermost atomic layers.[38] Jahn-Teller distortion (''tilting'') of the dimers can cause additional electron transfer into the upper silicon atom of the dimer pair, resulting in even stronger surface fields.[39,40] Monohydride termination redistributes charge into the bulk and symmetrizes the dimers,[40,41] thereby quenching the surface field[42] with only a slight effect on surface strain.[26] Dihydride termination breaks the dimer bond, thereby almost completely relaxing dimer-induced strain.[26] We therefore anticipate that variations in the second term in Eq. (1) dominate monohydride-induced SH spectroscopic effects, while variations in the first term dominate dihydride effects. Nevertheless the assumed separation of these terms is an approximation, since surface strain and electric fields are not entirely independent.[43]

Two additional SH polarizations have been omitted from Eq. (1) and will be neglected in this paper: (1) a bulk quadrupole polarization $\mathbf{P}^{\rm BQ}(2\omega)=\overleftrightarrow{\chi}_{\rm bulk}^{(2)Q}:\mathbf{E}(\omega)\nabla\mathbf{E}(\omega)$, a source distributed throughout the SH escape depth ($10<\delta_{\rm SH}<100$ nm depending on wavelength), and a region possessing the bulk O_h symmetry of silicon. One component of this term is distinguished by its fourfold anisotropic dependence on azimuthal crystal rotation.[37] Elsewhere[28] we show that the amplitude of the fourfold rotational component of the SH signal is only about one-tenth of the isotropic component at Si(001)-2×1 for wavelengths used in this study, and can be rendered negligible by choosing an incidence plane orientation for which it vanishes. There is also an isotropic component of $\mathbf{P}^{\rm BQ}(2\omega)$.[37] Because we have observed previously that the E_1 peak of the total field-independent isotropic contribution is strongly redshifted from its bulk energy,[27] this component is believed to be small with respect to the isotropic surface component. To the extent that it contributes, it will be incorporated into the first term in Eq. (1) in this paper. (2) A bulk EFISH polarization $\mathbf{P}^{\rm BE}(2\omega)=\overleftrightarrow{\chi}_{\rm bulk}^{(3)}:\mathbf{E}(\omega)\mathbf{E}(\omega)E_{\rm dc}^{\rm bulk}$ can also be neglected for low doping levels. At Si(001)-2×1 the Fermi level is pinned at 0.3 or 0.63 eV above the valence band for p and n type, respectively.[42] With an estimated unintentional doping level $<10^{15}$ cm^{-3} in our epitaxial film, the band bending is no more than 0.1 eV for either type of doping, while the thickness of the space-charge region is at least 10^{-4} cm, assuming a Schottky barrier model. Thus $E_{\rm dc}^{\rm bulk}<1$ kV/cm over the SH escape depth, whereas previous SH spectroscopy of a Si(001) metal-oxide-semiconductor (MOS) structure showed that bulk EFISH contributions are negligible compared to surface contributions for $E_{\rm dc}^{\rm bulk}<10$ kV/cm.[27] On the other hand, since $E_{\rm dc}^{\rm surf}$ exceeds $E_{\rm dc}^{\rm bulk}$ by 3–4 orders of magnitude, it can produce observable EFISH signals in spite of its 2–3 order of magnitude shorter spatial extent.

With these assumptions the magnitude of the total p-polarized SH field, $E_p(2\omega)=|\mathbf{E}_p(2\omega)|$, can be expressed as[37]

$$E_p(2\omega)=[(f_1\chi_{zzz}^{\rm eff}+f_2\chi_{xzx}^{\rm eff}+f_3\chi_{zxx}^{\rm eff})\cos^2\psi+f_4\chi_{zxx}^{\rm eff}\sin^2\psi]E^2(\omega), \tag{2}$$

where

$$\chi_{ijk}^{\rm eff}=\chi_{s,ijk}^{(2)}+\chi_{s,ijkz}^{(3)}\int_0^{+\infty}E_{\rm dc}^{\rm surf}(z)\exp(i\Delta z)dz \cong\chi_{s,ijk}^{(2)}+\chi_{s,ijkz}^{(3)}(E_{\rm dc}^{\rm surf})_{\rm eff}L_{\rm eff} \tag{2a}$$

represent the three effective nonvanishing, independent, nonlinear susceptibility tensor components $[ijk=zzz,xzx(=xxz),zxx]$,[18] f_n ($n=1,2,3,4$) are coefficients that contain the local field correction and Fresnel factors of the incoming fields,[18,37] ψ is the angle between the incident plane and the vector $\mathbf{E}(\omega)$ inside the sample, and $\Delta=(2\omega/c)[(n_\omega+ik_\omega)\cos\theta_\omega+(n_{2\omega}+ik_{2\omega})\cos\theta_{2\omega}]$, where n_i,k_i,θ_i are the refractive index, extinction coefficient, and refraction angle, respectively, at the fundamental ($i=\omega$) or SH ($i=2\omega$) frequencies. $\psi=0°$, 45°, and 90° correspond to p, q, and s fundamental polarizations, respectively. The middle expression of Eq. (2a) takes into account a small vertical spread of $E_{\rm dc}^{\rm surf}(z)$ over a thin surface region that has been assigned a uniform $\chi_s^{(3)}$. If $E_{\rm dc}^{\rm surf}(z)$ is approximated as a uniform field $(E_{\rm dc}^{\rm surf})_{\rm eff}$ extending to depth $L_{\rm eff}$ beneath the surface, then the simplified expression on the right side of Eq. (2a) is valid as long as $|\Delta|L_{\rm eff}\ll1$. This limit certainly holds for our wavelengths since $\delta_{\rm SH}\approx|\Delta|^{-1}\geq100$ Å, whereas $L_{\rm eff}$ is at most a few angstroms. When a strong bulk space charge field $E_{\rm dc}^{\rm bulk}$ is present, bulk EFISH field contributions of the form $E_p^{\rm BE}(2\omega)=f_5\chi_{{\rm bulk},ijkz}^{(3)}\int_0^{+\infty}E_{\rm dc}^{\rm bulk}(z)\exp(i\Delta z)dz$ are also present. When, as is commonly the case, $\delta_{\rm SH}$ is much less than depth W of the depletion field (e.g., $\delta_{\rm SH}\approx100$ Å near the E_1 resonance, $W\sim3000$ Å for the MOS structures used in Ref. 27), $E_p^{\rm BE}(2\omega)$ can be approximated as $f_5\chi_{{\rm bulk},ijkz}^{(3)}E_{\rm dc}^{\rm int}\delta_{\rm SH}$, analogous to the right-hand expression in Eq. (2a), where $E_{\rm dc}^{\rm int}$ is the value of the depletion field at the interface. Expressing $E_p^{\rm BE}(2\omega)$ in this form facilitates comparisons of bulk EFISH, surface EFISH, and field-independent surface contributions, as discussed further in Sec. IV.

The p-polarized second-harmonic intensity is

$$I_p(2\omega)\propto|\mathbf{E}_p(2\omega)|^2. \tag{3}$$

In this paper, we will present data taken using p-in/p-out configuration at a fixed sample azimuth. Since the SH signal for this configuration includes contributions from three independent effective susceptibility tensor components [see Eq. (2)], we have also measured the tenfold weaker SH signals generated in s-in/p-out and q-in/s-out configurations, which isolate the zxx and xzx components, respectively. From these measurements we determined that the $\chi_{zzz}^{\rm eff}$ component strongly dominates the p-in/p-out SH signal, confirming previous similar findings by others.[17]

The spectrum $I_{pp}(2\omega)$ of SH radiation in our wavelength range consists of a two-photon resonance peak at $2\hbar\omega\sim3.35$ eV from the surface-modified E_1 direct gap and a nonresonant background. For clean Si(001)-2×1, our background $I_{pp}(2\omega)$ is approximately 20% of the E_1 peak height intensity below resonance ($2\hbar\omega\sim3.0$ eV), then rises sharply

in magnitude above resonance ($2\hbar\omega > 3.45$ eV), suggesting that it originates primarily from a nearby higher-energy resonance. A background below the E_1 resonance with similar properties was reported by Daum *et al.* [see Fig. 2(e) of 17] for this surface. The existence of a broad higher-energy resonance that occurs around 3.6–3.8 eV, attributed to the disordering of the Si atoms at the interface, has recently been observed at oxidized Si(001).[44] Thus we shall represent our observed SH spectra phenomenologically by the expression

$$I_{pp}(2\omega) \sim \left| \frac{A}{2\omega - \omega_{\mathrm{SD}} + i\Gamma_{\mathrm{SD}}} + \frac{B}{2\omega - \omega_{\mathrm{SE}} + i\Gamma_{\mathrm{SE}}} + C(2\omega) \right|^2, \tag{4}$$

where the background term $C(2\omega)$ is the tail of a higher-energy resonance centered near 3.6 eV, and the E_1 resonance has been written as a sum of two Lorentzians representing surface dipole (SD) and surface EFISH (SE) contributions, respectively. This separation allows for the E_1 resonance of the SD contribution to differ slightly in frequency and broadening factor (Γ) from the SE contribution to optimize fits to the data. Physically, such a difference could arise if, for example, the former contribution is dominated by step edges and the latter by dimers on terraces and/or if the two polarizations differ in vertical spatial distribution. However, a rigorous physical interpretation of such differences will not be attempted in this paper.

A polarizable-bond model of SHG, advanced recently by Mendoza and Mochán,[30] is a promising future direction for a more complete theoretical description of the effects of H termination on SH spectroscopy of Si(001). In this formalism, surface EFISH effects would be described as changes in the nonlinear polarizability of surface bonds, while lattice distortions would change SHG via a nonlinear local field effect.

IV. RESULTS AND DISCUSSION

A. SH spectroscopy of isothermal and isosteric Si(001) surfaces

1. Temperature dependence of SH spectra: Clean Si(001)-2×1 and 1 ML H-Si(001)-2×1

Figure 1 shows a series of isothermal p-in/p-out SH spectra of the clean Si(001)-2×1 reconstructed surface, as determined by RHEED, at eight fixed temperatures ranging from 200 to 900 K. A broad peak, attributable to the two-photon E_1 resonance,[17] is evident in each spectrum. As the temperature increases this peak redshifts from about 3.4 eV (at 200 K) to 3.05 eV (at 900 K), and broadens. The solid curves are fits to each spectrum using Eq. (4) with a weak SD($A, \omega_{\mathrm{SD}}, \Gamma_{\mathrm{SD}}$) and strong SE($B, \omega_{\mathrm{SE}}, \Gamma_{\mathrm{SE}}$) resonant terms and background $C(2\omega)$ modeled as a Lorentzian peak centered near 3.6 eV. This model is discussed further in Sec. IV A 3 below. The resonant energy ($\hbar\omega_{\mathrm{SD,SE}} = E_1$) and broadening ($\Gamma$) parameters extracted from these fits have been plotted in Fig. 2 as filled squares and open circles, respectively. For comparison, the corresponding Lorentzian energy and broadening parameters of the E_1 critical point obtained by Lautenschlager *et al.*[25] from spectral ellipsometric analysis of bulk silicon have been plotted as dashed and dotted curves, respectively, in Fig. 2. The temperature-dependent

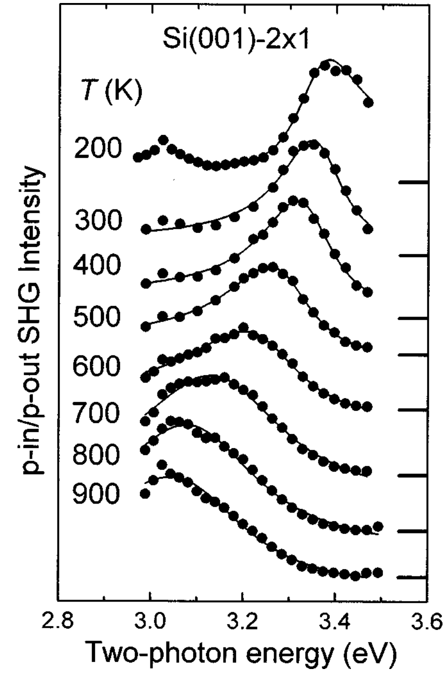

FIG. 1. Isothermal p-in/p-out SH spectra of a clean Si(001)-2×1 reconstructed surface. The broad peak is the E_1 two-photon resonance, which redshifts and broadens with increasing temperature. Solid curves are Lorentz oscillator model fits to the data as described in text. Bars on the right vertical scale indicate the corresponding zero SH intensity level.

resonant energies agree within experimental error. Our Γ parameters are approximately 30% smaller than the corresponding bulk parameters, but follow the same temperature coefficient within experimental error. A weak, narrow peak at temperature-independent two-photon energy $2\hbar\omega = 3.02$ eV is also evident in the spectra of Fig. 1.

Figure 3 shows a similar series of isothermal p-in/p-out SH spectra of 1-ML hydrogen-covered Si(001)-2×1, the reconstruction again confirmed by RHEED. For comparison, the SH response of the bare surface at 200 and 600 K are shown in the inset. In order to maintain constant monohydride coverage while acquiring these spectra, the temperature range was restricted from 200 to 600 K, since hydrogen desorbs too quickly above about 700 K. The two-photon E_1 resonance peak is also evident in these spectra, but with three differences from the corresponding clean surface spectra: (1) SH intensity at the peak is about three times weaker; (2) the peak is redshifted about 0.1 eV from its clean surface energy; (3) the line shape is asymmetrically distorted (enhanced from Lorentzian on the low-energy side, suppressed on the high-energy side). Apart from these differences, the redshift and broadening of the E_1 peak with increasing temperature closely resemble the behavior of the corresponding bare silicon spectra. Each spectrum was fit (solid curves) to Eq. (4) with the same SD and background $C(2\omega)$ terms as used in Fig. 1, but with a much weaker SE term. The underlying physical justification is discussed in Sec. IV A 3 below. The fitted resonant energy and broadening (Γ) parameters of the E_1 peak have been plotted in Fig. 2 as cross and plus symbols, respectively. Apart from the 0.1-eV redshift of the peak energy, the temperature dependence agrees with that of the bare surface within experimental error. The weak feature at

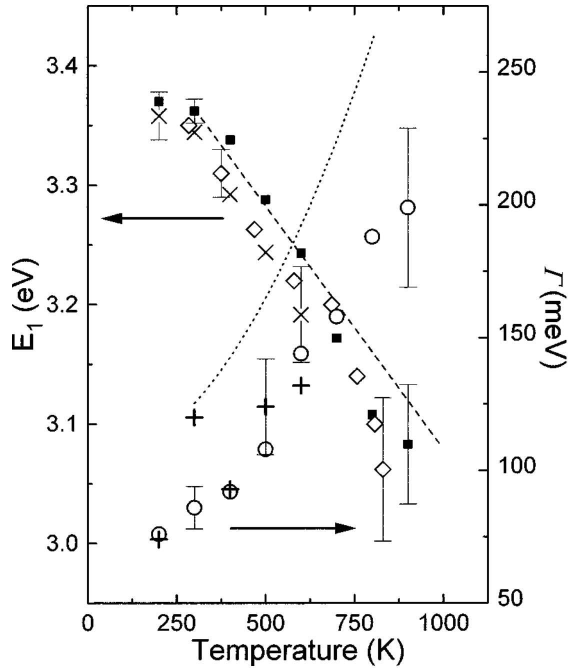

FIG. 2. Temperature-dependent E_1 resonant energy (left vertical scale) obtained from isothermal SH spectroscopy of clean Si(001)-2×1 (■) and H-Si(001)-2×1 surfaces (×), from single wavelength SH response during programmed heating (◇), and from bulk linear spectroscopy (dashed line). Temperature-dependent E_1 broadening coefficients (right vertical scale) obtained from isothermal SH spectroscopy of clean Si(001)-2×1 (○) and H-Si(001)-2×1 surfaces (+), and from bulk linear spectroscopy (dotted line).

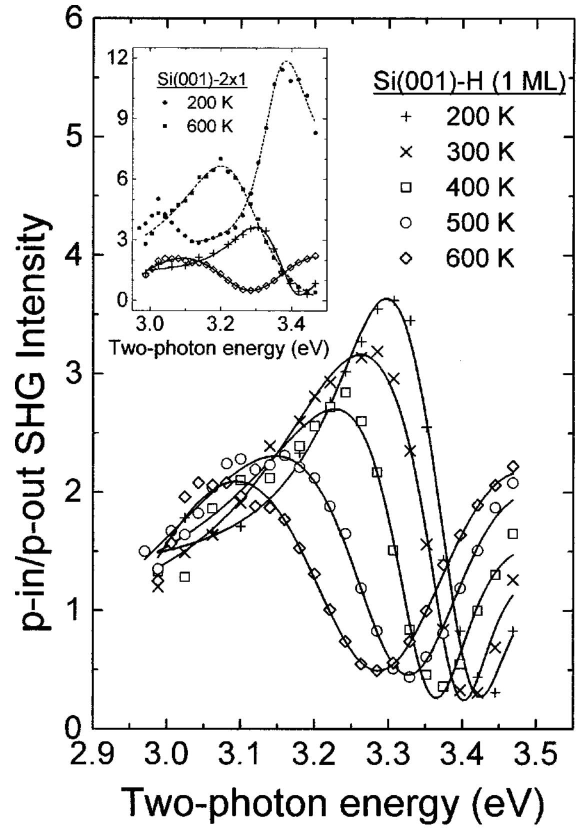

FIG. 3. Main panel: isothermal p-in/p-out SH spectra of a monohydride-terminated Si(001)-2×1 reconstructed surface. The broad peak is the E_1 two-photon resonance, which redshifts and broadens with increasing temperature. The resonances are weaker, redshifted, and asymetrically distorted compared to corresponding clean surface resonances shown in Fig. 1. Solid curves are Lorentz oscillator model fits to the data as described in text. Inset: comparison of isothermal SH spectra for bare and 1 ML H-terminated Si(001) at 200 and 600 K.

$2\hbar\omega = 3.02$ eV is completely quenched in the spectra of H-Si(001)-2×1.

2. H-coverage dependence of SH spectrum: Room temperature

Figure 4 (top panel) shows a series of room-temperature p-in/p-out SH spectra of Si(001) for ten H coverages ranging from 0 to 1.5 ML. As coverage Θ_H increases, three trends are evident: (1) from 0 to 1 ML the E_1 resonance is sharply quenched, while from 1 to 1.5 ML there is hardly any further decrease in its amplitude; (2) from 0 to 1 ML, the peak redshifts monotonically away from the peak energy at 0 ML, while from 1 to 1.5 ML, the peak blueshifts slightly back toward its 0-ML peak energy (3.36 eV); and (3) as the resonance quenches, its line shape distorts asymmetrically as a pronounced dip develops on its high energy side, as was shown in Fig. 3. RHEED patterns show that the dimerized 2×1 reconstruction persists for coverages up to 1 ML, and converts to 1×1 for higher coverages. The solid curves through each spectrum were fit to the data based on Eq. (4). The SD and SE Lorentz oscillators that underlie this fit are depicted in the bottom panel of Fig. 4. The $\Theta_H = 0$ ML spectrum was fit with the same Lorentzian oscillator model used to fit the 300-K spectrum of clean Si(001) in Fig. 1. Likewise the $\Theta_H = 1$ ML spectrum was fit with the same model used to fit the 300-K spectrum of H-Si(001) in Fig. 3. For intermediate coverages $0 < \Theta_H < 1.0$ ML, the SE oscillator strength B was decreased from $B(\Theta_H = 0\text{ ML})$ to $B(\Theta_H = 1\text{ ML})$, as depicted by the relative resonant peak heights shown in the bottom panel Fig. 4, with A, ω_{SD}, and ω_{SE} held constant. In addition slight adjustments to $C(2\omega)$ (not shown) were required to optimize the fits in this Θ_H range. For $1 \leqslant \Theta_H \leqslant 1.5$ ML, ω_{SD} was increased as indicated by the arrows in the bottom panel of Fig. 4 while other parameters remained at their $\Theta_H = 1$ ML values. The physical basis of these parameter variations is discussed below.

3. Discussion of isothermal and isosteric SH spectra

The E_1 critical point of bulk Si, which originates from Λ_3-Λ_1 electronic transitions, redshifts and broadens with increasing temperature because of the combined effect of lattice thermal expansion and electron-phonon interactions.[25] The quantitative agreement between its temperature shift and broadening coefficients[25] and those determined from the SH data in Figs. 1–3 suggests that their temperature shifts are of identical origin, and confirms the E_1 assignment of the SH peak. The lack of strong temperature dependence to the amplitude of the spectra in Fig. 1 justifies the neglect of the bulk EFISH mechanism. Since the bulk Fermi level depends strongly on temperature, while the surface Fermi level is nearly independent of temperature,[40] the temperature dependence of the band bending would cause modulations of the SH signal amplitude that are not observed. For example, for

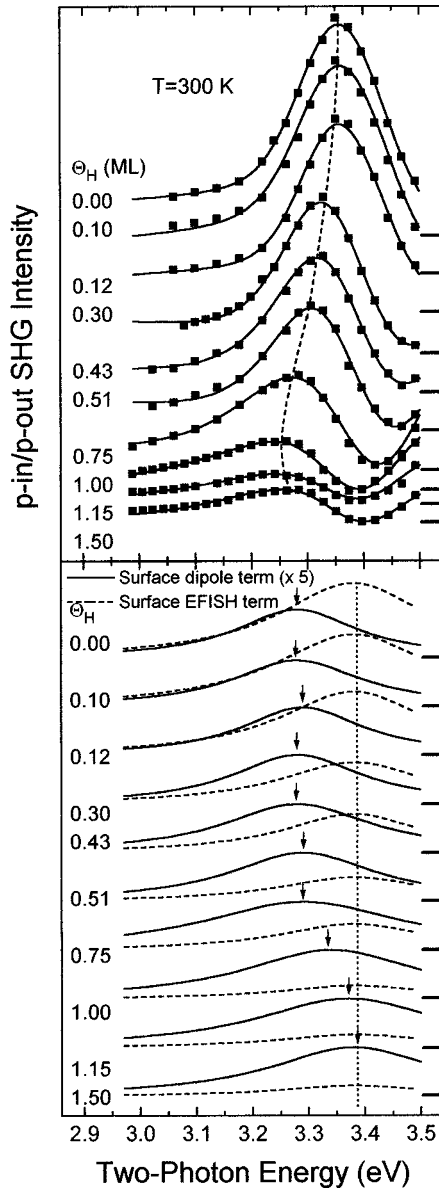

FIG. 4. Top panel: isothermal p-in/p-out SH spectra of 10 isosteric Si(001) surfaces with hydrogen coverages varying from 0 to 1.5 ML at room temperature. Note quenching, redshift (indicated by the dashed line through the SH peaks), and line shape distortion of E_1 resonance as coverage increases from 0 to 1.0 ML, and blueshift as coverage increases from 1.0 to 1.5 ML. Bottom panel: surface dipole and surface EFISH Lorentz oscillators underlying fit (solid curves) to top panel data. Note strong quenching of surface EFISH E_1 resonance (fixed at 3.38 eV indicated by the vertical dotted line), and nearly constant surface E_1 resonance (indicated by the arrows) between 0 and 1 ML; blueshift of surface resonance for $\geqslant$1 ML coverage. Bars on the right vertical scale indicate the corresponding zero SH intensity level.

p doping at $n_p = 10^{15}$ cm^{-3} the bulk Fermi level changes from 0.17 to 0.28 eV above the valence band as temperature changes from 200 to 300 K, changing band bending from 0.12 to 0.04 eV. This would cause a decrease of a factor of 3 in SH intensity if bulk EFISH were dominant, which is not observed.

The E_1 shifts induced by H coverage appear to be of less straightforward origin than those induced by temperature change. Daum *et al.*[17] proposed that the SH E_1 peak at clean Si(001)-2×1 acquires both its amplitude and redshift primarily from near-surface vertical tensile strain induced by the dimerized reconstruction, which enhances the surface dipole polarization[45] [first term in Eqs. (1) and (4)] and decreases the E_1 gap.[46] The complete quenching of the resonance by saturated H termination was invoked in support of this interpretation, since dihydride termination breaks the surface dimer bonds responsible for the 2×1 reconstruction.[4–8] The SH spectra presented in Fig. 4, by including finer increments in H coverage, now force us to revise this interpretation. Two observations are critical. First, the major influence of H on the SH E_1 peak occurs for $0 \leqslant \Theta_H \leqslant 1$ ML, where RHEED observations by us and others show[8,35] that the surface maintains its 2×1 dimerized reconstruction. Consequently, changes in atomic positions, and therefore strain, are minimal. On the other hand, dihydride termination ($\Theta_H > 1$ ML), which induces a much more drastic structural change,[4–8] affects the SH spectrum only slightly (see bottom three spectra in Fig. 4). Thus strain relaxation can hardly be the exclusive, or even primary, mechanism responsible for changing the SH spectrum. Secondly, the top eight spectra in Fig. 4 ($0 \leqslant \Theta_H \leqslant 1$ ML) show that monohydride termination redshifts the SH E_1 peak *away from* the bulk E_1 energy, contrary to the expected effect of relaxing near-surface tensile strain. The expected blueshift toward the bulk E_1 energy is weakly evident only in the bottom three spectra of Fig. 4, where such a strain relaxation is expected from dihydride termination. We must conclude that the much larger changes in the SH spectrum observed for $0 \leqslant \Theta_H \leqslant 1$ cannot be related simply to changes in subsurface strain.

On the other hand, the Fig. 4 data can be explained consistently by assuming that the SH E_1 peak at clean Si(001)-2×1 acquires most of its amplitude from the surface dc electric field [via the second term in Eq. (1)] associated with dimer bond formation[38] and tilting[39] rather than from the near-surface strain field. Energy minimization calculations[38] that predict a symmetric dimer structure indicate electron enrichment of approximately $e/6$ in the top two atomic layers, implying surface charge density $\sigma_s = 10^{-5}$ C/cm^2 and field strength on the order of $E_{\rm dc}^{\rm surf} \sim \sigma_s/\epsilon \sim 10^4$ kV/cm immediately beneath the surface, where the bulk dielectric constant $\epsilon = 11.9$ has been used as an approximation. Calculations that predict a tilted dimer indicate an even larger charge transfer of approximately $e/3$ into the upper silicon atom of each buckled dimer,[39] implying proportionately larger charge density and field strength in some portions of the immediate subsurface region, depending on details of the charge redistribution. Similar $E_{\rm dc}^{\rm surf}$ values and vertical extent are implied by the decrease of 0.35 eV of the ionization energy of the Si(001)-2×1 surface, which is observed when monohydride termination passivates and symmetrizes the surface dimer and quenches the surface field.[42] The latter result implies $(E_{\rm dc}^{\rm surf})_{\rm eff} L_{\rm eff} = 0.35$ V, a parameter [see Eq. (2a)] that is proportional to the surface EFISH component $\mathbf{E}_p^{\rm SE}(2\omega)$ of the total surface SH field $\mathbf{E}_p(2\omega)$. To compare $\mathbf{E}_p^{\rm SE}(2\omega)$ to the bulk EFISH field $\mathbf{E}_p^{\rm BE}(2\omega)$ measured in a Si(001) MOS structure[27] and to the field-independent component of the surface SH field, we assume $\chi_s^{(3)} \approx \chi_{\rm bulk}^{(3)}$, $f_1 \approx f_5$, and $\chi_s^{(2)}[{\rm Si}(001)/{\rm SiO}_2] \approx \chi_s^{(2)}$

$\times$[Si(001)-2$\times$1], In the MOS structure measurements, SH signals near the E_1 resonance were enhanced approximately fourfold over their flat-band values—the same enhancement observed at the clean, compared to the monohydride-terminated, Si(001)-2$\times$1 surface—when the MOS structure was externally biased approximately 1 V from flat-band condition. This bias corresponded to a depletion field $E_{\rm dc}^{\rm int} \approx 10^5$ V/cm immediately beneath the Si/SiO_2 interface for the structures used.[47] Since $\delta_{\rm SH} \approx 100$ Å near the E_1 resonance, the bulk EFISH signal responsible for this enhancement is proportional to $E_{\rm dc}^{\rm int}\delta_{\rm SH} \approx 0.1$ V, the same order of magnitude as $(E_{\rm dc}^{\rm surf})_{\rm eff}L_{\rm eff} = 0.35$ V at the clean Si(001)-2$\times$1 surface. This approximate comparison demonstrates that surface EFISH associated with surface dimer formation and buckling can produce the observed SH signal enhancement at the clean Si(001)-2$\times$1 surface.

The above interpretation does not, of course, rule out the existence of direct monohydride-induced alterations to the field-independent component $\chi_s^{(2)}:\mathbf{E}(\omega)\mathbf{E}(\omega)$ of the surface nonlinear polarization, which can be caused either by altering the energy of surface dimer electronic bands[32] or by changing subsurface equilibrium atomic structure. However, available calculations together with the experimental evidence presented above suggest that both of these effects on the SH spectrum are smaller than the surface EFISH effect. Self-consistent tight-binding calculations for Si(001)-2$\times$1 show that significant resonant enhancements of $\chi_{s,zzz}^{(2)}$ attributable to surface dimer bands occur only at photon energies ($1.0 < 2\hbar\omega < 3.0$ eV) lower than those used in the current study.[32] At these infrared photon energies, the calculated $\chi_{s,zzz}^{(2)}$ is indeed sensitive to monohydride termination,[32] and will be an interesting subject of future experiments. However, in our current photon energy range, $\chi_{s,zzz}^{(2)}$ derives entirely from surface projections of bulk bands, and is therefore insensitive to surface dimer bands and monohydride termination. Regarding changes in subsurface structure, an energy minimization calculation based on a three-layer cluster with fixed Si-Si back bond lengths[26] showed that monohydride termination of clean Si(001)-2$\times$1 alters the dimer bond length by less than 3% with no perceptible change in subsurface Si-Si bond angles. Dihydride termination, on the other hand, by breaking the dimer bond, increases the separation of the surface Si atoms by over 70% with significant alteration of subsurface Si-Si bond angles.[26] Although a self-consistent calculation of hydrogenated Si(111) (Ref. 43) has shown that H-induced electronic charge transfer, similar to that which accompanies monohydride termination of Si(001)-2$\times$1, can induce slight changes in Si-Si back bond lengths, monohydride-induced changes of the structure of Si(001)-2$\times$1 are clearly negligible in general compared to those induced by dihydride termination.[26] Since we observe the latter to influence the SH spectrum only slightly, we must conclude that monohydride-induced subsurface relaxation, though present, affects $\chi_{s,zzz}^{(2)}$ even less than the much larger dihydride-induced subsurface relaxation. Thus the charge-transfer effect (i.e., surface EFISH) must dominate over structural effects in determining SH spectral properties during monohydride termination of Si(001)-2$\times$1. In fitting the Fig. 4 data with Eq. (4), we are therefore justified in holding the surface dipole oscillator strength (A) and frequency ($\omega_{\rm SD}$) constant over the range $0 \leq \Theta_{\rm H} \leq 1$ ML.

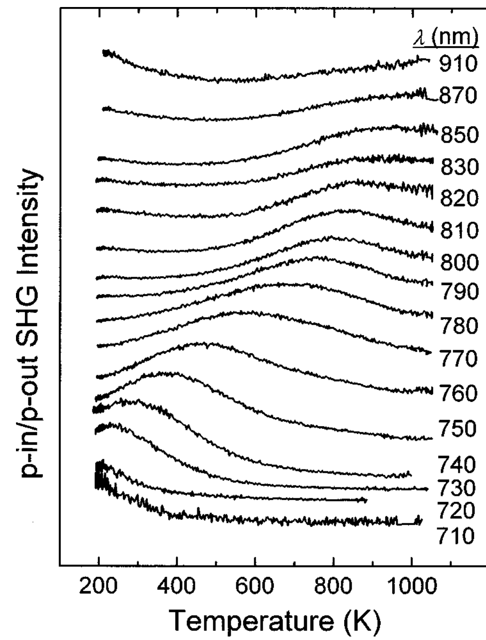

FIG. 5. A series of fixed wavelength p-in/p-out SH responses of a clean Si(001)-2$\times$1 surface as temperature is ramped upward at 2 K/s. The broad peaks results from the E_1 resonance thermally redshifting through the fixed two-photon energy. Each SH trace is vertically offset for clarity.

The relationship between the redshift and line-shape distortion of the surface resonance deserves brief comment. The E_1 redshifts observed in several recent SH spectroscopic studies of Si-SiO_2,[27,44,48,49] reconstructed Si(001),[17,50] and Si(111)-7$\times$7 (Ref. 17) interfaces in some cases implied local volume expansion far exceeding that produced by known interfacial bond distortion mechanisms.[17,51] The weak spectral blueshift that we observe upon increasing $\Theta_{\rm H}$ from 1 to 1.5 ML (Fig. 4) suggests that intrinsic tensile strain exists and does contribute to the surface E_1 redshift. However, the line-shape distortion evident in the $\Theta_{\rm H} = 1$ ML scans of Figs. 3 and 4 demonstrates that interference between resonant E_1 and nonresonant background contributions creates an additional redshift that augments the intrinsic shift. Such apparent peak shifts are well known in nonlinear spectroscopy.[29] In the present case, the off-resonant contribution to the surface $\chi_{s,zzz}^{(2)}$ [$C(2\omega)$ term in Eq. (4)] originate from electronic resonances at higher energy than the surface-modified E_1 resonance. Thus below the surface E_1 energy ($2\omega < \omega_{\rm SD}$), the resonant (first) and nonresonant (last two) terms in Eq. (4) are in phase and constructively interfere, while above resonance ($2\omega > \omega_{\rm SD}$), they are out of phase and destructively interfere, simultaneously creating the apparent redshift of the surface resonance peak $\hbar\omega_{\rm SD}$ and an asymmetric line-shape distortion in $I_{pp}(2\omega)$. Since the weaker surface dipole resonance (dominant for 1 ML coverage) is comparable in magnitude to the nonresonant background, it is more strongly influenced by the interference than the stronger surface EFISH resonance (dominant for 0 ML). The Lorentz oscillator fit to the Fig. 4 data reproduces these trends, and shows that the peak SH signal for the 1 ML case is redshifted 0.04 eV from the true surface resonance energy ($\hbar\omega_{\rm SD}$) by

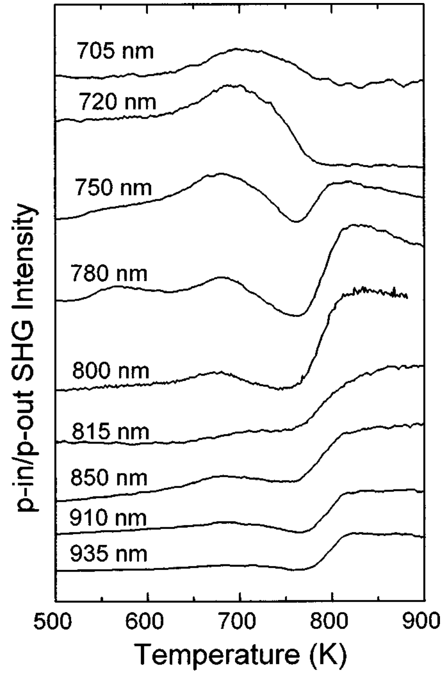

FIG. 6. A series of fixed wavelength p-in/p-out SH responses of an initially hydrogen-saturated ($\Theta_H = 1.5$ ML) Si(001) surface as temperature is ramped upward at 2 K/s. $\beta 2$ desorption rate is maximum between 600 and 700 K, β_1 desorption rate between 700 and 850 K. Each SH trace is vertically offset for clarity.

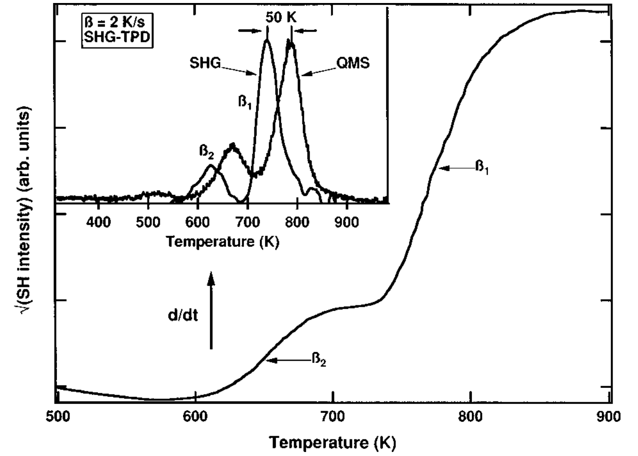

FIG. 7. Main panel: square root of p-in/p-out response at 200 mW average power, $\lambda = 815$ nm, during temperature-programmed desorption. Inset: time derivative of square root of SH response at $\lambda = 815$ nm, compared to quadrupole mass spectrometer data. Note good agreement of β_2 and β_1 relative peak heights, with 50 K temperature offset due to laser heating.

the interference mechanism described above. Thus an intrinsic shift of approximately 0.08 ± 0.02 eV from strain and other mechanisms is also present.

The weak resonant feature at $2\hbar\omega = 3.02$ eV (see Fig. 1) has not been identified. Its temperature independence and sensitivity to H coverage suggest that it involves one- ($\hbar\omega = 1.51$ eV) or two-photon transitions between surface states. Single-photon transitions at $\hbar\omega = 1.15$ and 1.3 eV between the rest atom and adatom dangling bond states at the clean Si(111)-7$\times$7 have recently been reported.[20]

B. SH monitoring of transient phenomena at Si(001) surfaces

1. Programmed heating of clean Si(001)-2×1

Figure 5 shows the p-in/p-out SH response of clean Si(001)-2$\times$1 at a series of fixed wavelengths ranging from 710 to 910 nm as temperature is ramped linearly at 1 K/s from 200 to 1000 K. For each wavelength a broad peak occurs at a particular temperature $T_{\max}$. This peak shifts to higher temperatures as the wavelength is increased. These wavelengths (converted to two-photon energies) have been plotted against the corresponding $T_{\max}$ as open diamonds in Fig. 2. The resulting plotted points coincide, within experimental error, with the temperature-dependent two-photon E_1 peaks (filled squares in Fig. 2) extracted from the isothermal SH spectra of clean Si(001)-2$\times$1 (Fig. 1). Hence we conclude that this feature results from the temperature shift of the E_1 resonance through the fixed two-photon energy. Two additional features from Fig. 5 data are noteworthy. First, at the shorter wavelengths (710–720 nm), the SH signal is nearly temperature independent at temperatures $T > 500$ K. This feature is advantageous in studies of hydrogen desorption dynamics described below. Secondly, at the longer wavelengths ($810 \leqslant \lambda \leqslant 910$ nm), the SH signal decreases as temperature increases from 200 to 400 K. This feature, unrelated to the E_1 resonance, may be caused by incipient formation of a new low-temperature surface reconstruction;[52] however, it plays no role in the studies described below. All features shown in Fig. 5 are reproduced when the direction of the temperature ramp is reversed.

2. Temperature-programmed hydrogen desorption

Figure 6 shows the p-in/p-out SH response of initially H-saturated Si(001) at a series of fixed wavelengths ranging from 705 to 935 nm as temperature is ramped linearly at 2 K/s from 500 to 900 K. During this ramp Θ_H decreases monotonically from 1.5 to 0 ML. On the other hand, most of the SH responses are not monotonic. Some (e.g., 780 nm) display complicated oscillations and are convolved responses to simultaneous changes in substrate temperature and H coverage. Nevertheless, the 815-nm SH signal does increase monotonically in two discernible steps reminiscent of the β_2 (dihydride) and β_1 (monohydride) hydrogen desorption features. Moreover the short wavelength (705–720 nm) response, although not monotonic, varies quite strongly at the temperatures (600–800 K) where most of the hydrogen is desorbing; this temperature dependence is connected solely with hydrogen desorption since the bare surface SH response is invariant with temperature (Fig. 5). These two responses were therefore investigated in greater detail as promising candidates for real-time SH probing of H coverage.

In Fig. 7 (main panel) the dynamic 815-nm SH response obtained with 200-mW average incident laser power is plotted on an expanded vertical scale. In the inset of Fig. 7, the time derivative of the smoothed square root of the SH intensity $[\propto |\mathbf{P}(2\omega)|]$ is plotted and compared to the hydrogen desorption rate monitored by a differentially pumped QMS. The SH derivative signal shows two well-defined peaks with the same relative amplitudes and temperature separation as the well-known β_2 and β_1 desorption features evident in the

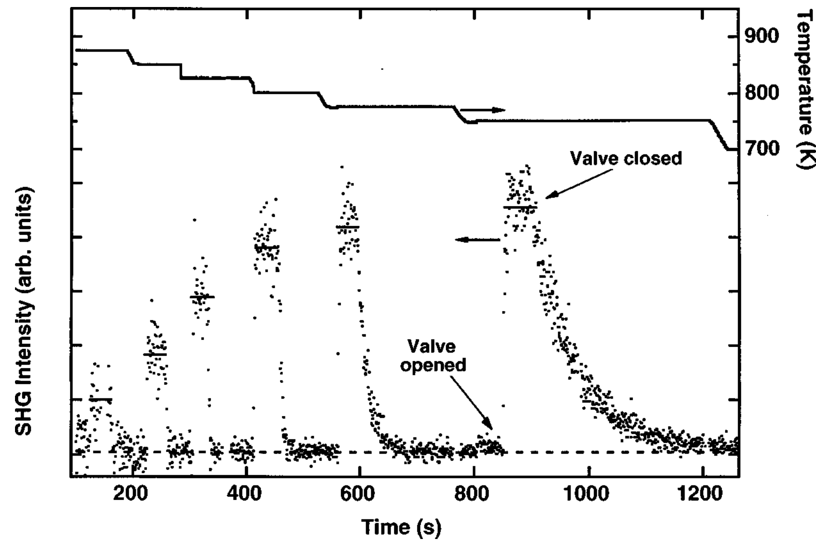

FIG. 8. A series of p-in/p-out SH responses of an initially clean Si(001)-2×1 surface using 715 nm fundamental wavelength as disilane pressure in the growth chamber is periodically modulated at several different substrate temperatures. Note rapid (<0.2 s) rise time of each pulse, corresponding to disilane adsorption; temperature-dependent fall times, corresponding to isothermal hydrogen desorption; temperature-dependent plateau levels, corresponding to epitaxial growth.

QMS data. However, they are shifted about 50 K lower in temperature, as monitored by a thermocouple several mm away from the illuminated spot on the crystal. As the average power of the fundamental beam is attenuated, however, the temperature of the desorption features shifts up linearly toward the QMS response at a rate of approximately 0.2 K/mW. For example, at incident average laser powers of $\leqslant 50$ mW we have obtained a SH derivative scan that, although noisier, yields β_2 and β_1 desorption peaks nearly coincident with the QMS data. The cumulative steady-state local heating of the photoexcited area introduced by linear absorption of the 815-nm light has been calculated by solving the thermal diffusion equation,[23] and agrees with the temperature offsets shown in Fig. 7 (inset). We conclude that the temperature offsets are caused by local laser heating of the surface not detected by the thermocouple. The temperature scale of Fig. 6 (but not Fig. 7) has been corrected for this measured laser-induced temperature offset. This local heating is a shortcoming of our current monitoring laser, but not a fundamental limitation of the SH monitoring technique. The laser heating can be reduced substantially by shortening the laser pulse duration to 30–50 fs,[53] cavity dumping the laser,[54] or scanning the silicon surface[23] without sacrificing SH signal ($\propto \tau^{-1}$). The similarity of the QMS and SH derivative curves in Fig. 7 (inset) demonstrates that the square root of the 815-nm SH intensity can monitor Θ_H on Si(001) in real time (0.1-s resolution) from 0 to 1.3 ML with an estimated accuracy of 5% over a temperature range from 600 to 900 K.

3. *Epitaxial growth*

The short wavelength (705–720 nm) SH signals (see top two traces in Fig. 6) increase monotonically in the β_2 desorption range (600–700 K), decrease monotonically in the β_1 desorption range (700–850 K), and maintain temperature-independent plateau levels outside these temperature ranges. This observation suggests their utility as H coverage monitors within the ranges $1.5 > \Theta_H > 1$ ML or $1 > \Theta_H > 0$ ML. Here we illustrate the use of 715-nm SH signals to monitor Θ_H between 0 and 1 ML ($875 > T > 750$ K) during isothermal disilane adsorption and hydrogen desorption, which accompany epitaxial film growth via CVD.

Figure 8 shows the raw 715-nm SH data obtained by modulating the pressure of disilane at a series of decreasing substrate temperatures (solid line, right axis). At the rising edge of each pulse in Fig. 8, a valve was opened to backfill the chamber to 5×10^{-4} Torr total pressure (4% disilane/helium mixture), causing H coverage and SH intensity to rise within 0.2 s to a steady-state level, corresponding to the coverage at which the rates of disilane adsorption and hydrogen desorption balance. While the valve is open, an epitaxial silicon film is growing. When the valve is closed, the disilane partial pressure falls at approximately 2 decades per second to its residual gas analysis (RGA) detection limit ($< 1 \times 10^{-12}$ Torr), resulting in a decrease at the trailing edge of each pulse that is determined by the rate of hydrogen desorption.

As substrate temperature decreases from 875 to 750 K (left to right in Fig. 8), two trends are evident: (1) the SH signal at the trailing edge of each pressure pulse falls more slowly, as a result of slower H_2 desorption; (2) the steady-state SH signal during epitaxial growth increases, as a result of higher steady-state hydrogen coverage caused by slower H_2 desorption. Consistent with these trends, we observe that SH intensity is unperturbed by pressure modulation at $T > 900$ K, suggesting that the steady-state hydrogen coverage becomes vanishingly small (the growth is adsorption limited under these conditions). For $T < 750$ K, the steady-state hydrogen coverage saturates at 1 ML (where the growth rate is desorption limited). Throughout the sequence of pressure pulses shown in Fig. 8, the background 715-nm SH signal before and after each pulse (corresponding to a bare surface) remains at a nearly constant level, even though the temperature decreases and the film thickness increases.

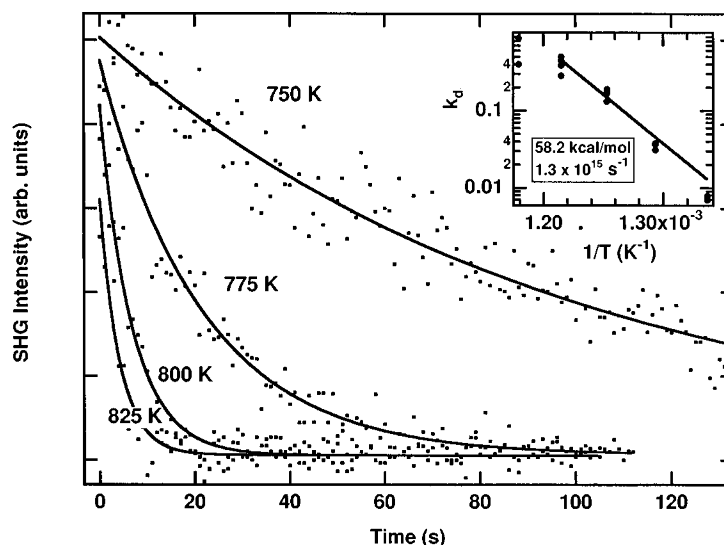

FIG. 9. Main panel: detail of desorption transients at 4 different substrate temperatures from SH data at 715 nm fundamental wavelength. Solid curves are fits of data to exponential decay curves, which assume first-order desorption kinetics. Inset: Arrhenius plot of desorption rate constant. Solid line is a fit to the data, and corresponds to the activation energy and preexponential factor given in the box.

Figure 9 shows a series of desorption transients from the trailing edges of the pressure pulses in Fig. 8 in greater detail. Assuming first-order desorption kinetics, which is approximately valid for $\Theta_H > 0.1$ ML,[13] a series of exponential decay curves were fit to the data (solid lines) using $I(2\omega) \propto |\Theta_H|^2 \propto |\exp(-k_d t)|^2$. Desorption rate constants obtained in this manner are plotted in an Arrhenius fashion in the inset of Fig. 9, including a 50-K temperature offset in the reciprocal temperature scale, as described earlier. The Arrhenius plot is somewhat sublinear, probably because the first-order model does not fit the high-temperature and low-coverage data. However, the magnitude of the activation energy, 2.53 eV (58.2 kcal/mol), and preexponential factor, 1.3×10^{15} s^{-1}, compare favorably to published values for the monohydride desorption kinetics.[13,55]

Variations in the backfill pressure help to calibrate the vertical scale of Fig. 8 in terms of H coverage. For example, by increasing the pressure to 100 mTorr, we observed no further increase in the 715-nm SH intensity beyond the level approached in the 775-K and 750-K pulses shown in Fig. 8. This demonstrates that this SH signal corresponds to $\Theta_H \approx 1$ ML, with growth rate controlled by the monohydride desorption kinetics. We rule out the possibility of a significant dihydride population under these conditions, as the dihydride desorption kinetics are too fast at these temperatures. We further rule out a submonolayer saturation of the SH intensity, as there is no time lag between the cessation of the pressure pulse, and the onset of the SH desorption transient.

Results qualitatively similar to those shown in Fig. 8 were obtained for $\lambda = 815$ nm. However, the strong temperature dependence of the SH intensity from both the bare and hydrogen-covered surfaces complicate quantitative analysis, since the effects of temperature and hydrogen coverage must be deconvolved.

4. *Discussion of real-time, fixed wavelength SH measurements*

The 815-nm SH signal is, like most of the signals shown in Fig. 6, a convolved response to H coverage and temperature during temperature-programmed H_2 desorption. Specifically, the first ''step'' of the 815-nm ($2\hbar\omega = 3.04$ eV) SH response shown in Fig. 7 is caused by the redshift of the E_1 resonance, which in turn is caused partly by the increased surface dimerization strain accompanying the β_2 hydrogen desorption (evident in the bottom 3 traces of Fig. 4) and partly by the thermal redshift accompanying the increase in temperature from 600 to 700 K (evident in Figs. 1 and 3). The strong second ''step'' of the response is caused partly by the growth of the electric-field-induced contribution accompanying the β_1 hydrogen desorption (the effect evident in the top 7 traces of Fig. 4) and partly by continuing thermal E_1 redshift. As the TPD experiment represents only a single ''curve,'' $\Theta_H(T)$ in the two-dimensional Θ_H-T parameter space, the simple proportionality of the 815-nm SH intensity to H coverage (apparent in Fig. 7) masks the complicated temperature and coverage dependence of the 815-nm SH response evident in isothermal and isosteric studies between 700 and 900 K. On the other hand the 705–720-nm ($2\hbar\omega > E_1$ for $T > 700$ K) signal appears selectively sensitive to H coverage and insensitive to temperature changes for $0 < \Theta_H < 1$ ML and $700 < T < 900$ K. Thus it proves more versatile as a monitor of the complex adsorption and/or desorption dynamics involved in epitaxial growth. Use of infrared femtosecond sources[56] may provide additional opportunities for monitoring H coverage by exploiting electronic resonances from surface dimer bands[32] or Si-H vibrational resonances.[15,57]

These studies point to several conclusions regarding SH monitoring of H coverage during CVD. First the SH signals should initially be independently calibrated using QMS and pressure variation techniques such as those described above. Secondly, a tunable laser source such as Ti:sapphire offers flexibility in finding effective monitoring wavelengths at which adsorption, desorption, and growth dynamics can be monitored over significantly larger Θ_H and T ranges than achieved in past SH studies with fixed wavelength lasers.[13] Thirdly, complete SH spectroscopic databases that track the

dependence of the contributing susceptibilities on temperature, Θ_H, doping, and alloy material composition—of which Figs. 1 and 3–5 represent a beginning—must be compiled, analogous to dielectric function databases, which underlie ellipsometric analysis of growth surfaces.[19] Femtosecond lasers provide the data acquisition speed and tunability required for such compilations. In addition, by monitoring changes in H coverage with <0.1-s resolution, SHG can provide an early warning of changes in growth rate, and thus may provide a useful error signal in active feedback control of CVD growth.

V. CONCLUSION

We have presented a comprehensive SH spectroscopic study of the Si(001) surface in the presence of calibrated variations of temperature and hydrogen coverage. A Ti:sapphire femtosecond laser provided wide tunability ($0.7<\lambda<1.0\,\mu$m), high SH signal acquisition rate ($>10^3$ counts/s), and low surface heating (<50 K). The principal spectroscopic finding on isothermal-isosteric surfaces was the strong quenching, redshift, and line-shape distortion of the two-photon E_1 resonance, which occurred as hydrogen coverage increased from 0 to 1 ML, when structural modifications to the dimerized 2×1 reconstruction were negligible. Based on this finding, we proposed that surface electric fields associated with dimer formation and tilting, rather than strain, were the dominant source of p-polarized SH from the clean Si(001)-2×1 surface, and that monohydride termination quenched this contribution through chemical modification of the surface. SH spectroscopic consequences of strain relief were weakly evident only at coverages (>1 ML) at which dimer bonds were broken. Thermal shifts of E_1 and line-shape distortions from interference between resonant and off-resonant SH sources were also clearly evident in the isothermal and isosteric surface spectroscopy.

We then demonstrated two wavelength ranges in which SH could dynamically monitor H coverage during temperature-programmed hydrogen desorption or epitaxial film growth over much larger coverage ranges than were achieved in previous SH studies with fixed frequency lasers. The real-time SH signals were calibrated by QMS measurements of desorption products, and yielded kinetic rate constants for hydrogen desorption in good agreement with independent measurements. The results demonstrate the potential of femtosecond-laser-generated SH for applications to real-time monitoring of epitaxial growth by chemical vapor deposition.

ACKNOWLEDGMENTS

We acknowledge useful discussions with M. McEllistrem and technical assistance from R. Barber. This work was supported by the NSF Science and Technology Center Program (CHE-8920210), the Office of Naval Research (ONR N00014-91-J1513), the Texas Advanced Technology Program (ATPD-354), the Air Force Office of Scientific Research (AFOSR Contract F49620-95-C-0045), AFOSR/ DARPA Multidisciplinary University Research Initiative (Contract F49620-95-1-0475), and the Robert Welch Foundation (F-1038).

*Present address: Department of Chemistry and Department of Physics, Columbia University, New York, NY 10027.

†Present address: Applied Materials, Inc., 3100 Bowers Ave., M/S 0225, Santa Clara, CA 95054.

‡Present address: Texas Instruments, Inc., 13536 N. Central Expressway, Dallas, TX 75265.

[1] B. A. Joyce and R. R. Bradley, J. Electrochem. Soc. **110**, 1235 (1963).

[2] Ch. Kleint, B. Hartmann, and H. Meyer, Z. Phys. Chem. (Leipzig) **250**, 315 (1972).

[3] Y. I. Belyakov, N. I. Jonov, and T. N. Komponits, Fiz. Tverd Tela (Leningrad) **14**, 2992 (1972) [Sov. Phys. Solid State **14**, 2567 (1973)].

[4] H. Ibach and J. E. Rowe, Surf. Sci. **43**, 481 (1974).

[5] T. Sakurai and H. D. Hagstrum, Phys. Rev. B **14**, 1593 (1976).

[6] Y. J. Chabal, Surf. Sci. **168**, 594 (1986).

[7] L. S. O. Johansson, R. I. G. Uhrberg, and G. V. Hansson, Surf. Sci. **189/190**, 479 (1987).

[8] J. J. Boland, Phys. Rev. Lett. **65**, 3325 (1990).

[9] L. C. Feldman, P. J. Silverman, and I. Stensgaard, Nucl. Instrum. Methods **168**, 589 (1980).

[10] C. M. Greenlief and M. Armstrong, J. Vac. Sci. Technol. B **13**, 1810 (1995).

[11] T. F. Heinz, M. M. T. Loy, and S. S. Iyer, Mat. Res. Soc. Symp. Proc. **75**, 697 (1987).

[12] R. W. J. Hollering, A. J. Hoeven, and J. M. Lenssinck, J. Vac. Sci. Technol. A **8**, 3194 (1990).

[13] P. Bratu and U. Höfer, Phys. Rev. Lett. **74**, 1625 (1995); U. Höfer, L. Li, and T. F. Heinz, Phys. Rev. B **45**, 9485 (1992); G. A. Reider, U. Höfer, and T. F. Heinz, J. Chem. Phys. **94**, 4080 (1991); G. A. Reider, U. Höfer, and T. F. Heinz, Phys. Rev. Lett. **66**, 1994 (1991).

[14] T. F. Heinz, M. M. T. Loy, and W. A. Thompson, Phys. Rev. Lett. **54**, 63 (1985).

[15] P. Guyot-Sionnest, P. Dumas, and Y. J. Chabal, J. Electron Spectrosc. Relat. Phenom. **54/55**, 27 (1990).

[16] H. B. Jiang, Y. H. Liu, X. Z. Lu, W. C. Wang, J. B. Zheng, and Z. M. Zhang, Appl. Phys. Lett. **65**, 1558 (1994); Phys. Rev. B **50**, 14 621 (1994).

[17] W. Daum, H.-J. Krause, U. Reichel, and H. Ibach, Phys. Scr. **T49**, 513 (1993); Phys. Rev. Lett. **71**, 1234 (1993).

[18] Y. R. Shen, Nature (London) **337**, 519 (1989); Y. R. Shen, *The Principles of Nonlinear Optics* (Wiley, New York, 1994).

[19] D. E. Aspnes, Surf. Sci. **307-309**, 1017 (1994), and references therein.

[20] K. Pedersen and P. Morgen, Phys. Rev. B **52**, R2277 (1995).

[21] T. Suzuki and Y. Hirabayashi, Jpn. J. Appl. Phys., Part 2 **32**, L610 (1993); OSA Tech. Digest Series **12**, 141 (1993).

[22] U. Höfer, L. Li, E. H. Ratzlaff, and T. F. Heinz, Phys. Rev. B **52**, 5264 (1995).

[23] J. I. Dadap, X. F. Hu, N. M. Russell, J. G. Ekerdt, J. K. Lowell, and M. C. Downer, IEEE J. Sel. Top. Quantum Electron. **1**, 1145 (1995).

[24] G. A. Reider and T. F. Heinz, in *Photonic Probes of Surfaces*, edited by P. Halevi (Elsevier, Amsterdam, 1995), p. 413.

[25] P. Lautenschlager, P. B. Allen, and M. Cardona, Phys. Rev. B **31**, 2163 (1985); **33**, 5501 (1986).

[26]Z. Jing and J. L. Whitten, Phys. Rev. B **46**, 9544 (1992).
[27]J. I. Dadap, X. F. Hu, M. H. Anderson, M. C. Downer, J. K. Lowell, and O. A. Aktsipetrov, Phys. Rev. B **53**, R7607 (1996).
[28]Z. Xu, X. F. Hu, D. Lim, J. G. Ekerdt, and M. C. Downer, J. Vac. Sci. Technol. B **15**, 1059 (1997); D. R. Aktsipetrov, A. A. Fedyanin, A. V. Melnikov, J. I. Dadap, X. F. Hu, M. H. Anderson, M. C. Downer, and J. K. Lowell, Thin Solid Films **294**, 231 (1997).
[29]R. P. Chin, J. Y. Huang, Y. R. Shen, T. J. Chuang, H. Seki, and M. Buck, Phys. Rev. B **45**, 1522 (1992).
[30]B. S. Mendoza and W. L. Mochán, Phys. Rev. B **53**, R10 473 (1996); **55**, 2489 (1997).
[31]L. Reining, R. Del Sole, M. Cini, and J. G. Ping, Phys. Rev. B **50**, 8411 (1994).
[32]V. I. Gavrilenko and F. Robentrost, Appl. Phys. A: Solids Surf. **60**, 143 (1995).
[33]B. K. Kellerman, A. Mahajan, N. M. Russell, J. G. Ekerdt, S. K. Banerjee, A. F. Tasch, A. Campion, J. M. White, and D. J. Bonser, J. Vac. Sci. Technol. A **13**, 1819 (1995).
[34]J. T. Law, J. Chem. Phys. **30**, 1568 (1959); G. Schulze and M. Henzler, Surf. Sci. **124**, 336 (1983).
[35]S. Asami, N. M. Russell, A. Mahajan, P. A. Steiner, D. J. Bonser, J. Fretwell, S. Bannerjee, A. Tasch, J. M. White, and J. G. Ekerdt, Appl. Surf. Sci. **82/83**, 359 (1994).
[36]S. M. Gates, R. R. Kunz, and C. M. Greenlief, Surf. Sci. **207**, 364 (1989).
[37]H. W. K. Tom, T. F. Heinz, and Y. R. Shen, Phys. Rev. Lett. **51**, 1983 (1983); J. E. Sipe, D. J. Moss, and H. M. van Driel, Phys. Rev. B **35**, 1129 (1987); O. A. Aktsipetrov, I. M. Baranova, and Yu. A. Il'inskii, Zh. Eksp. Teor. Fiz. **91**, 287 (1986) [Sov. Phys. JETP **64**, 167 (1986)].
[38]B. I. Craig and N. V. Smith, Surf. Sci. **218**, 569 (1989).
[39]D. J. Chadi, Phys. Rev. Lett. **43**, 43 (1979); W. X. Verwoerd, Surf. Sci. **99**, 581 (1980).
[40]W. Mönch, *Semiconductor Surface and Interfaces*, 2nd ed. (Springer-Verlag, Berlin, 1995), and references therein.
[41]T. Uchiyama and M. Tsukada, Surf. Sci. Lett. **295**, L1037 (1993).
[42]P. Koke and W. Mönch, Solid State Commun. **36**, 1007 (1980); W. Mönch, P. Koke, and S. Krueger, J. Vac. Sci. Technol. **19**, 313 (1981).
[43]E. Kaxiras and J. D. Joannopoulos, Phys. Rev. B **37**, 8842 (1988).
[44]W. Daum (private communication).
[45]S. V. Govorkov, V. I. Emel'yanov, N. I. Koroteev, G. I. Petrov, I. L. Shumay, and V. V. Yakovlev, J. Opt. Soc. Am. B **6**, 1117 (1989).
[46]N. V. Nguyen, D. Chandler-Horowitz, P. M. Amirtharaj, and J. G. Pellegrino, Appl. Phys. Lett. **64**, 2688 (1994); J. T. Fitch, C. H. Bjorkman, G. Lucovsky, F. H. Pollak, and X. Yin, J. Vac. Sci. Technol. B **7**, 775 (1989).
[47]O. A. Aktsipetrov, A. A. Fedyanin, J. I. Dadap, and M. C. Downer, Laser Phys. **6**, 1142 (1996).
[48]C. Meyer, G. Lüpke, U. Emmerichs, F. Wolter, H. Kurz, C. H. Bjorkman, and G. Lucovsky, Phys. Rev. Lett. **74**, 3001 (1995).
[49]P. Godefroy, W. de Jong, C. W. van Hasselt, M. A. C. Devillers, and Th. Rasing, Appl. Phys. Lett. **68**, 1981 (1996).
[50]J. R. Power, J. D. O'Mahony, S. Chandola, and J. F. McGilp, Phys. Rev. Lett. **75**, 1138 (1995).
[51]E. Kobeda and E. A. Irene, J. Vac. Sci. Technol. B **7**, 163 (1989).
[52]N. Roberts and R. J. Needs, Surf. Sci. **236**, 112 (1990); J. Dabrowski and M. Scheffler, Appl. Surf. Sci. **56-58**, 15 (1992); R. A. Wolkow, Phys. Rev. Lett. **68**, 2636 (1992).
[53]M. T. Asaki, C. P. Huang, D. Garvey, J. Zhou, H. C. Kapteyn, and M. M. Murnane, Opt. Lett. **18**, 977 (1993).
[54]M. S. Pshenichnikov, W. P. de Boeij, and D. A. Wiersma, Opt. Lett. **19**, 572 (1994).
[55]N. M. Russell and J. G. Ekerdt, Surf. Sci. **369**, 51 (1996); **364**, 199 (1996).
[56]G. Lenz, W. Gellermann, D. J. Dougherty, K. Tamura, and E. P. Ippen, Opt. Lett. **21**, 137 (1996).
[57]M. Morin, P. Jakob, N. J. Levinos, Y. J. Chabal, and A. L. Harris, J. Chem. Phys. **96**, 6203 (1992).